



HAL
open science

Comparison of microstructure features and mechanical properties for additive manufactured and wrought nickel alloys 625

J. Nguejio, Fabien Szmytka, S. Hallais, A. Tanguy, S. Nardone, M. Godino
Martinez

► To cite this version:

J. Nguejio, Fabien Szmytka, S. Hallais, A. Tanguy, S. Nardone, et al.. Comparison of microstructure features and mechanical properties for additive manufactured and wrought nickel alloys 625. *Materials Science and Engineering: A*, 2019, 764, pp.138214. 10.1016/j.msea.2019.138214 . hal-03244530

HAL Id: hal-03244530

<https://hal.science/hal-03244530v1>

Submitted on 1 Jun 2021

HAL is a multi-disciplinary open access archive for the deposit and dissemination of scientific research documents, whether they are published or not. The documents may come from teaching and research institutions in France or abroad, or from public or private research centers.

L'archive ouverte pluridisciplinaire **HAL**, est destinée au dépôt et à la diffusion de documents scientifiques de niveau recherche, publiés ou non, émanant des établissements d'enseignement et de recherche français ou étrangers, des laboratoires publics ou privés.

Comparison of microstructure features and mechanical properties for additive manufactured and wrought nickel alloys 625

J. Nguejio^a, F. Szmytko^{1a}, S. Hallais^b, A. Tanguy^b, S. Nardone^c, M. Godino Martinez^c

^a*Institute for Mechanical Science and Industrial Application - CNRS, EDF, CEA, ENSTA Paris, Institut Polytechnique de Paris 828 Boulevard des Maréchaux 91762 Palaiseau - France*

^b*Laboratoire de Mécanique des Solides - UMR 7649 - Ecole Polytechnique 91128 Palaiseau - France*

^c*Engie LABORELEC, Rodestraat 125 1630 Linkebeek, Belgium*

Abstract

The microstructure characteristics as well as the mechanical properties of an Inconel 625 alloy obtained by three processes: forging, SLM and LMD, are investigated. For the last two processes, known as "additive manufacturing", the influence of printing parameters is considered as well as the role of possible heat treatments. First, microstructural analyses (SEM and EBSD) underline the presence of columnar dendrites with a very heterogeneous grain size for additive manufactured as-built materials. The microstructures appear highly textured, particularly for SLM ones which are also often finer than the ones obtained by LMD. Heat treatments and particularly a 1h-1100°C annealing is proven to improve the printed parts microstructure and to avoid a drastic decrease in terms of ductility, particularly for LMD parts. The LMD process with controlled laser power, coupled with appropriate heat treatment, finally produces materials with both microstructures and tensile mechanical properties close to or better than those of the wrought alloy.

Keywords: Nickel Superalloy, Selective Laser Melting, Laser Melting Deposition, Microstructure, Thermal treatments, Hardness, Tensile properties

¹Corresponding author: fabien.szmytko@ensta-paristech.fr

1. Introduction

Inconel alloy 625 is used extensively in different fields such as aerospace, chemical, petrochemical and marine industries. This material has shown good mechanical performances for components exposed in severe environments, including high temperature strength, high creep and high temperature corrosion resistances [1, 2, 3, 4].

Inconel 625 is a nickel-based superalloy mainly strengthened by the solid-solution hardening effect of elements such as niobium (Nb) and molybdenum (Mo) in a nickel-chromium matrix. After various thermal aging, this alloy was proved to be sensitive to the precipitation of strengthening intermetallic phases such as γ'' (Ni_3Nb) and δ (Ni_3Nb), to carbides (MC , M_6C) and to minor precipitations (Laves particles, Ti-rich particles, etc.) [3, 4, 5]. Extensive characterizations of wrought Inconel 625 have been performed in order to understand the effect of microstructure evolutions through the precipitation of γ'' and δ phases on the mechanical properties such as hardness and tensile strengths. These investigations reveal that Inconel 625 mechanical properties are greatly improved after annealing of samples for a temperature range between 650-900°C and for length well-above than 1 hour. This improvement is highlighted by the precipitation of hardening phases (γ'' and δ) in the nickel-chromium matrix. Over this temperature range, the mechanical properties decrease with the increasing of the annealing temperature [5, 6].

Therefore, the mechanical properties of this material could be subjected to great variations due to the thermal exposure and the effect of manufacturing processes, implying severe thermal gradients and variations, should be considered with care in terms of microstructure features and mechanical properties. Distinct from the conventional machining processes, that use subtractive methods (SM), additive manufacturing (AM) technologies offer the possibility to more easily create components with highly complex shapes at reduced costs. The common AM technologies used to create parts from metallic powders induce laser melting processes such as the Selective Laser Melting (SLM) and the Laser Melting Deposition (LMD). Both of these AM technologies produce 3-D printed parts directly from CAD (Computer-Aided-Design) models, in a layer by layer mode using laser energy. There are however some differences, especially on how the powder is carry onto the manufacturing substrate. On one hand, for the SLM process, a layer of powder is spread on a support, to be selectively melted by a focused

38 high-energy laser beam, according to a pre-determined pattern in the CAD data.
39 This process is then automatically repeated with a new layer of powder, spread
40 over the previous layers, and again melted, until the printing of the 3-D part is
41 completed. On the other hand, for the LMD process, the high-energy laser beam
42 and the metallic powder combined with a neutral gas- are simultaneously deliv-
43 ered into the melt pool on the substrate by a coaxial nozzle. The nozzle serves
44 to have the powder flows converge at the same point on the focused laser beam.
45 During the LMD manufacturing, the coaxial nozzle system moves along the x-y
46 plane, to build the surface of the pre-defined geometry; and then, the nozzle incre-
47 ment z, is applied to heighten the structure and create the 3-D parts.

48
49 Manufacturing processes similar to LMD have been known with different
50 names such as Laser Rapid Manufactured (LRM), Direct Energy Deposition (DED),
51 Laser Engineering Net Shaping (LENS), and other names, depending on the man-
52 ufacturers [7]. The LMD technologies offer many advantages including surface
53 coatings and repairs of damaged components by using the laser cladding process
54 [7, 8]. Generally, it is difficult to compare LMD and SLM technologies, because
55 they are complementary. Indeed, the SLM process allows the production of very
56 complex components with a higher dimensional accuracy [9], and less porosity
57 than the LMD one [13]. However, the LMD process is faster than the SLM one
58 and can be used to build wider components, in reason of the extended dimensions
59 of the building chamber. Therefore, the process choice depends on the industrial
60 application that is being targeted and also of the material mechanical properties.

61
62 The use of the high-energy laser beam results of a very high cooling rate dur-
63 ing the deposition/melting process, which affects the microstructure of the re-
64 sulting parts [8, 9, 10, 11, 12]. Concerning the Inconel 625 obtained by SLM,
65 observations reveal huge differences in terms of microstructure compared to the
66 well-known equilibrium structure of the wrought materials. Recent studies also
67 revealed that the high cooling rate, which occurs mostly via the substrate, leads
68 to a directional grains growth and afterwards the formation of elongated colum-
69 nar grains[10, 11, 12]. The grains growth direction is mostly perpendicular to the
70 substrate, and a build direction anisotropy is observed.

71
72 In the case of LMD parts, a dendritic microstructure is also observed by other
73 authors in nickel-based superalloys [7, 10, 13]. As a consequence, for both LMD
74 and SLM processes, the laser-printed parts exhibit a strong texture anisotropy that
75 has a significant effect on the mechanical properties. However, the reported val-

76 ues of yield strength (YS) and ultimate tensile strength (UTS), for both additive
77 manufacturing processes, are higher than the ones observed for wrought Inconel
78 625[12, 13, 14, 15]. Depending of the industrial application and the correspond-
79 ing mechanical loadings amplitude and directions, the strong texture of these parts
80 could reduce the mechanical resistance in lifetime operation, with the appearance
81 of a sudden brittle fracture of the material. Therefore, it may be necessary to
82 study the effect of heat treatments on the microstructure and mechanical proper-
83 ties of the SLM and LMD parts. Dinda et al. studied for instance the effects of
84 thermal treatment on the dendritic microstructure of Inconel 625 obtained by di-
85 rect energy deposition (DED) [7]. The dendritic microstructure modification was
86 only observed after a heat treatment above 1000°C , characterized by the recrystal-
87 lization (equiaxed) of some grains. Microhardness measurements were therefore
88 done to study the effect of these changes on the mechanical properties but tensile
89 tests were not performed. In recent studies, the effect of heat treatment on the
90 microstructure and hardness of SLM Inconel 625 parts were also studied to lead
91 to better isotropic mechanical properties[12, 16]. As example, Li et al. found a
92 homogeneous microstructure and weak texture for samples heat treated at 1150°C
93 [12]. Effects of heat treatments on the tensile mechanical properties have not yet
94 be investigated.

95
96 Impact of the post processing heat treatments on the tensile properties of SLM
97 Inconel 625 were investigated in recent papers. These investigations showed a
98 decrease of the mechanical strengths, following to the increase of the ductility, as
99 the recrystallization annealing was done around 1000°C [16, 17]. However, stud-
100 ies about the microstructural evolution under different heat treatments of laser-
101 powder deposited Inconel 625 parts, and its effect on the hardness and tensile
102 properties are quite uncommon. In addition, a direct extended comparison, using
103 exactly the same protocols, of the microstructural and mechanical properties (in-
104 cluding tensile tests) of Inconel 625 parts built by these two widely-used additive
105 manufacturing processes have been rarely performed. Therefore, we seek in this
106 present paper to characterize the microstructure features and mechanical proper-
107 ties of components obtained by LMD and SLM processes, and compare them to
108 the conventional wrought Inconel 625. The microstructural evolution under heat
109 treatments will be revealed by Scanning Electron Microscopy (SEM) observa-
110 tions, coupled with crystallographic and grain morphology textures analyses ob-
111 tained by Electron Backscatter Diffraction (EBSD). The microhardness and tensile
112 properties will be investigated to highlight the effect of annealing treatments and
113 how to reach an equilibrium grain structure in order to obtain properties similar to

114 those of the wrought Inconel 625.

115 **2. Material and experimental procedures**

116 *2.1. Material and processes*

Ni	Cr	Mo	Fe	Nb	C	Mn	Si	Al	Ti	P	S
Base	22	9	4	3.5	0.025	0.40	0.40	0.40	0.40	0.010	0.010

Table 1: Chemical composition of wrought Inconel 625 (% in weight)

117 As a reference material and a basis for comparison, we use a wrought Inconel
118 625, supplied by Goodfellow. The as-received wrought material was pre-annealed
119 at 900°C during several hours in order to stabilize the microstructure. Its chemical
120 composition is indicated in Table 1.

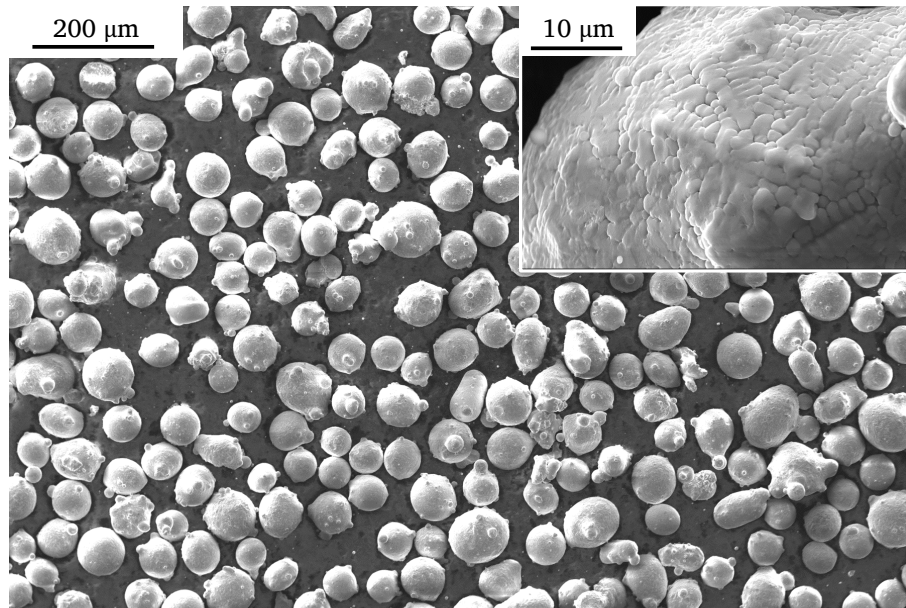


Figure 1: SEM morphology of Inconel 625 powder for LMD, with the upper inset showing micro-dendritic microstructure

121 A commercial Inconel 625 powder was supplied by Oerlikon (MetcoClad625)
122 for LMD process and its composition is reported in Table 2. Figure 1 shows the

123 SEM view, illustrating the powder size and morphology. The shape is practically
 124 spherical (with some satellites) and the interval particle size is 45-90 μm . The in-
 125 set in Figure 1 shows the internal microdendritic structure of the powder particle,
 126 which characterizes the austenitic γ phase growth.

Ni	Cr	Mo	Nb	Fe	Other
55.0 – 63.0	20.0 – 23.0	8.0 – 10.0	3.0 – 5.0	5.0	2.0

Table 2: Inconel 625 powder nominal chemical composition (% in weight)

128 LMD parts were fabricated on a BeAM Mobile machine developed by BeAM
 129 Company, France, now property of AddUp company. The LMD setup consists of
 130 a 500-W fiber laser, associated with a co-axial powder-feeding nozzle and a 5-axis
 131 workstation. A defocused laser beam spot was used for powder deposition, and
 132 a 30% overlapping ratio between adjacent laser scans was adopted. Argon was
 133 used as protective and powder carrier gas. 316L stainless steel 10mm-thick plates
 134 are chosen as substrates. The chosen scanning strategy is bidirectional, with a 90°
 135 rotation of the laser beam after each deposition as seen on Figure 2.

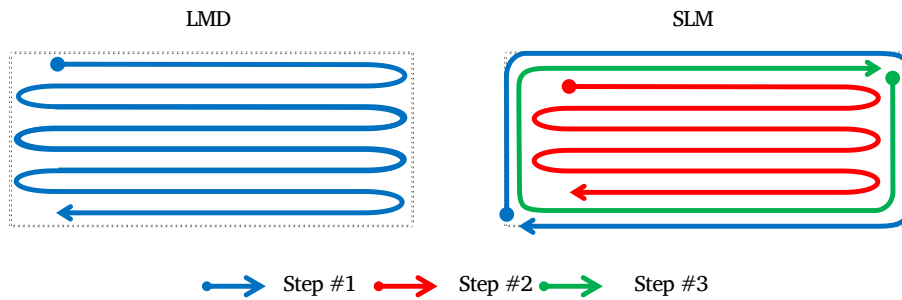


Figure 2: Layer deposition strategy for LMD and SLM built volumes

136 The output features of the process such as the height and the width of the laser-
 137 deposited layer seem strongly dependent on the laser melting deposition (LMD)
 138 parameters [18]. The more influent processing parameters on the laser clad char-
 139 acteristics are the laser power P (W), the scan speed V (mm/min), and the powder
 140 feed rate Q (g/min). The parameters used in this study to build LMD samples are
 141 reported in Table 3

Main parameters	Values	Fixed parameters	Values
P (W)	270, 300, 330	Laser spot (mm)	0.7
V (mm/min)	2000, 2500	Overlapping (%)	30
Q (g/min)	7	Z increment (mm)	0.2

Table 3: Process parameters values used to build LMD parts.

142 Another commercial Inconel 625 powder was supplied by LPW Technology
143 (LPW625) for SLM process and its composition is identical as the one reported
144 in Table 2. Powder particles are also spherical and their size ranges between 10
145 and 45 μm . The SLM parts have been produced using the Realizer SLM125 ma-
146 chine installed at ENGIE Laborelec’s premises. The optimized processing param-
147 eters were adopted for the built Inconel 625 parts, with a laser power of 247W, a
148 scan speed of 1000mm/s, a hatching distance of 0.08mm and a layer thickness of
149 0.2mm. Once again the scanning strategy is illustrated on Figure 2. The building
150 platform was kept at 100°C to reduce the residual stresses between the substrate
151 and the sample. Inconel 625 bars ($12 \times 12 \times 70\text{mm}^3$) were fabricated by both SLM
152 and LMD processes. The rectangular bars were horizontally printed, parallel to
153 the XY plane as seen on Figure 3.a.

154 2.2. *Experimental protocols*

155 Cubic samples were sectioned from rectangular parts and prepared to study
156 the microstructural features. They were polished with SiC paper up to grade 4000,
157 then with diamond paste down to 1 μm . The polished specimens were then electro-
158 etched for 1-3 minutes under 5 V potential, in a solution of 70 mL phosphoric acid
159 and 30 mL water, to highlight the microstructure.

160
161 Microstructures were then observed thanks to a digital microscope (Keyence
162 VHX 1000) and a Field Emission Gun - Environmental Scanning Electron Micro-
163 scope (FEG-ESEM - FEI Quanta 600). EBSD maps with an area of $1.5 \times 1.5\text{mm}^2$
164 and a pitch of 1.5 μm were obtained under 25 keV and a spot size of 4.5 (equiva-
165 lent to a 0.47 nA probe current) with a Nordlys II camera. The post processing of
166 these maps was done with CANNEL 5 software (Oxford Instruments) in order to
167 follow the crystallographic and grain morphology textures evolutions (grain size,
168 orientation) after heat treatments.

169
170 To study the effect of the thermal post-treatment on the microstructure, the

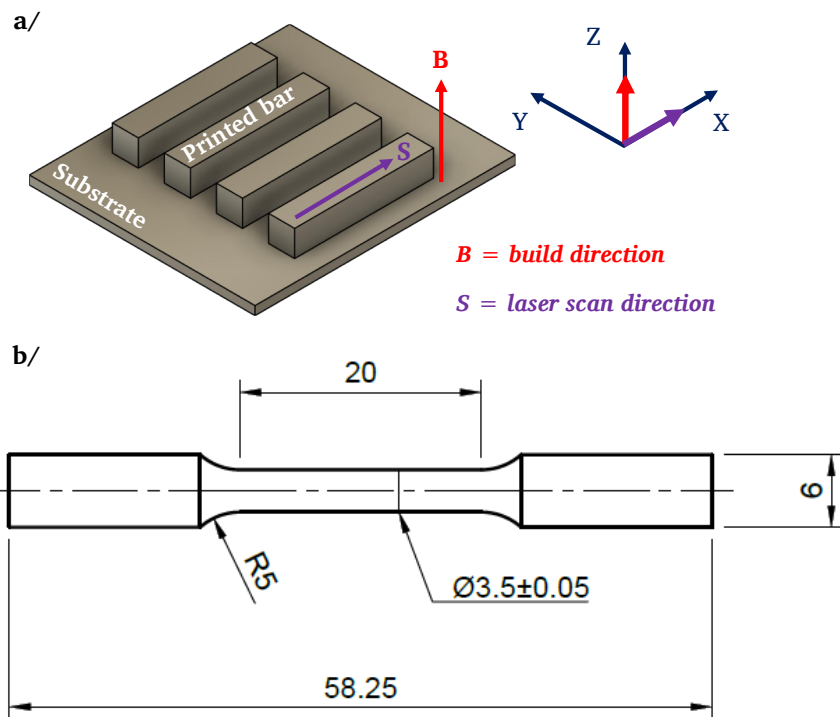


Figure 3: a. Illustration of the rectangular bars, printed by the SLM and LMD processes; b. Geometry of the tensile test specimens, obtained from printed rectangular bars ($70 \times 12 \times 12 \text{mm}^3$)

171 as-built samples were annealed respectively at 600, 700, 900, 1100°C for 1 hour
172 followed by cooling in air. The lattice parameters, useful to indirectly identify
173 the phase transformations, were measured using a X-ray diffractometer by Cu K α
174 radiation at 40 kV and 100 mA. The standard scanning $\theta - 2\theta$ geometry was done
175 for all samples from 20°C to 120°C with a 0.01°C step size and 1s dwell time.

176

177 The hardness was measured using a Vickers microhardness tester (Mitutoyo,
178 MVK-H1), applying a 0.5kg load for a dwell time of 15s. The final hardness value
179 was obtained by averaging data from twelve indentations on each sample. Tensile
180 tests were finally performed at room temperature, under a constant strain rate of
181 $10^{-3}s^{-1}$ using an Instron 5960 dual column tabletop testing system and a 30kN
182 load cell. Tensile specimens were machined from horizontal rectangular bars ($12 \times$
183 $12 \times 70mm^3$) according to the geometry specified on Figure 3.b for both LMD and
184 SLM processes, following ISO 6892-1 standard recommendations. Specimens
185 orientation was chosen to characterize tensile properties perpendicular to the build
186 direction and some specimens were heat-treated before tensile tests at 900°C and
187 1100°C during one hour into a primary vacuum furnace (10^{-2} mbar), to study
188 the thermal post-treatment effects on the mechanical properties. At least three
189 specimens were tested for each condition to assure statistical representativeness.

190 **3. Results and analyses**

191 *3.1. Microstructure characterization*

192 *3.1.1. Inconel 625 obtained by SLM process*

193 Figure 4 show the transverse section images of Inconel 625 obtained from
194 the SLM process. The microstructure of SLM parts frequently exhibits traces of
195 melt pools, created during the laser beam scanning. The shape and the width
196 of these melt pools depend on the adopted laser scan strategy. The nearly "V"
197 shape is attributed to the Gaussian distribution of the laser energy, with the high-
198 est value focused on the center of the laser beam [10]. The microstructure consists
199 on columnar dendrites as a result of the cooling that mostly occurs via the sub-
200 strate and the deposit. The heat flux direction during the solidification of the melt
201 pool thus enforces the vertical growth of the grains which appear nearly perpen-
202 dicular to the substrate.

203

204 This very fine microstructure can be observed by SEM, as shown in Figure
205 5. Two kinds of dendritic shape structures can here be observed: cellular-shaped
206 structures, and elongated dendrites, generally called "primary dendrites". These

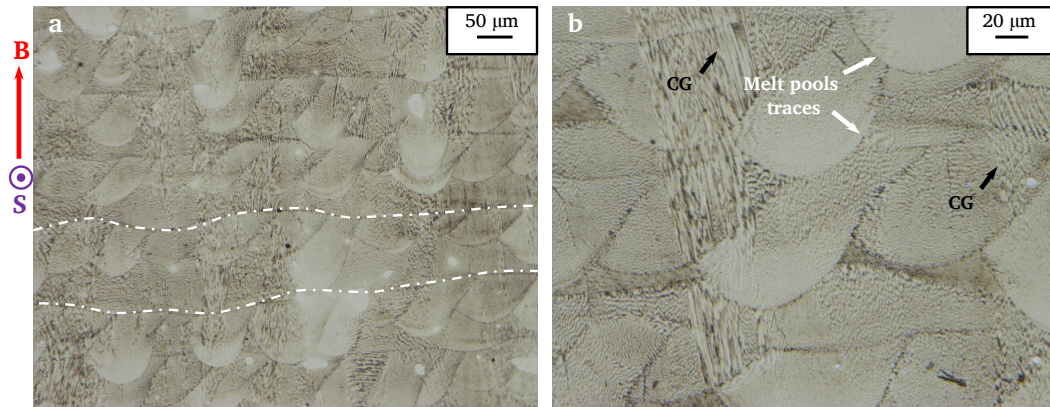


Figure 4: a. Optical micrograph of Inconel 625 processed by SLM at different magnifications (dotted lines are added to emphasize the layers); b. Optical micrograph of Inconel 625 processed by SLM at different magnifications(CG = columnar dendrites) - B stands for Building direction and S for Laser scan direction

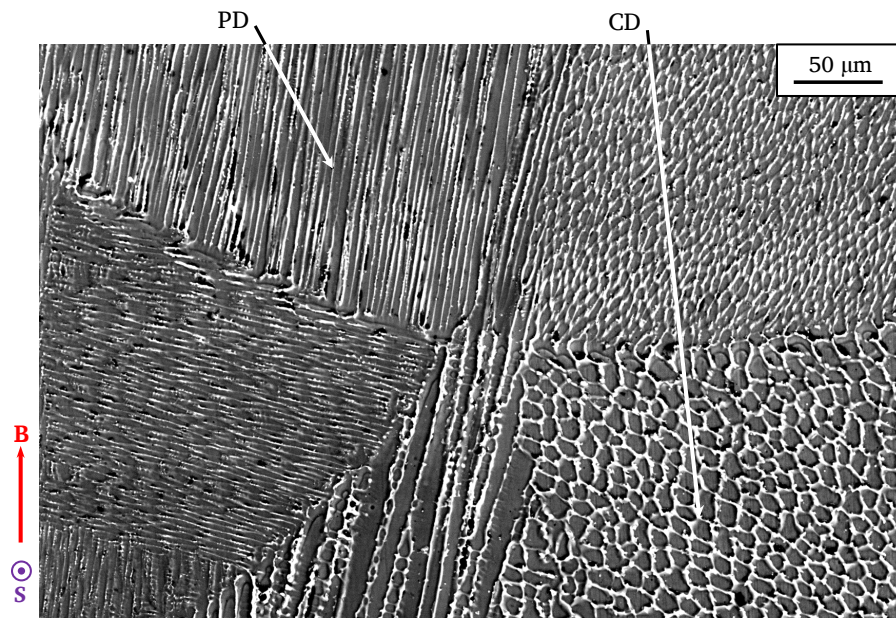


Figure 5: SEM images of Inconel 625 processed by SLM (PD = primary dendrites; CD = cell-like dendrites)- B stands for Building direction and S for Laser scan direction

207 latter grow in different orientations, depending on the main heat flux direction.
 208 Furthermore, the same dendritic structures are observed in the literature on the
 209 same kind of material by others researchers [10, 11, 16].

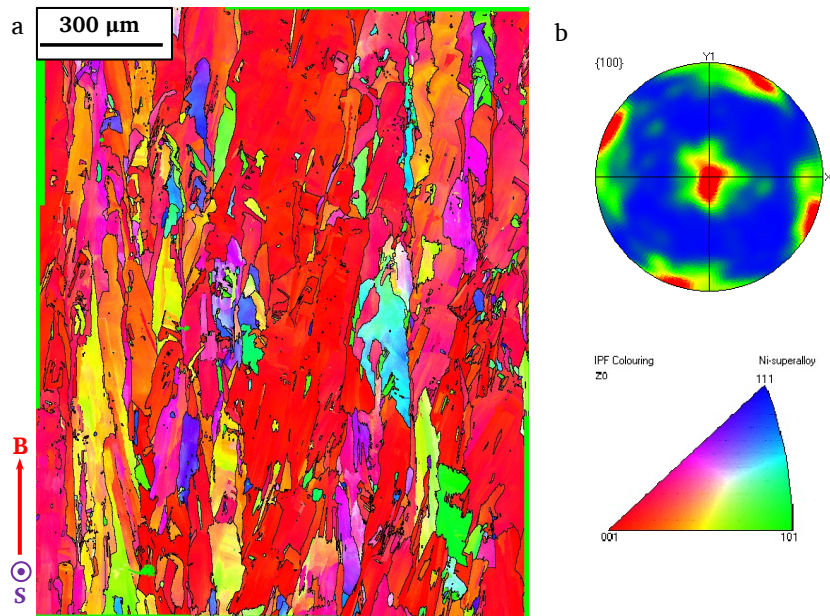


Figure 6: Microstructure of the SLM formed Inconel 625 from EBSD analyses: a. inverse pole figure (IPF-Z) colored map of the Y-Z section; b.(100) pole figure of the map - B stands for Building direction and S for Laser scan direction

210 EBSD analyses help to reveal the grains crystallography and morphology struc-
 211 ture of the as-built materials on Figure 6. The pole figure corresponding to the
 212 Y-Z section map exhibits a very strong texture for the SLM sample, quite simi-
 213 lar to standard observations for single crystals. This result can also be predicted
 214 with the very dominating red color of the IPF-Z colored map. Indeed, grains are
 215 aligned along the Z-direction, in consequence of the vertical high cooling flux,
 216 which occurs through the building platform. Therefore, the grains grow mostly
 217 from the substrate towards the melt pool boundary in a columnar structure. The
 218 preferential orientation of the grains is found to $\langle 001 \rangle$. This typical texture for
 219 the Inconel 625 obtained by the SLM process has previously been observed for
 220 similar material [11].

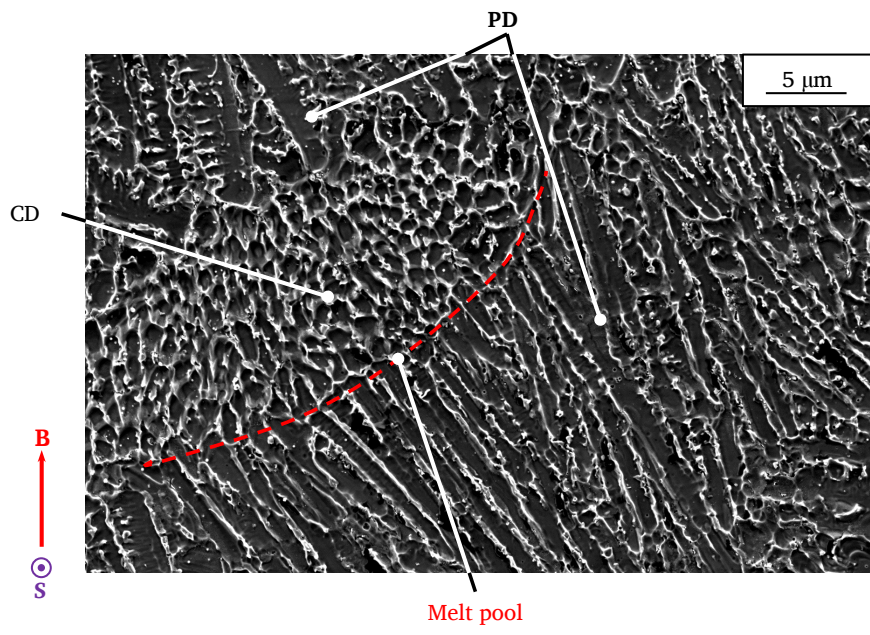


Figure 7: SEM images of Inconel 625 processed by LMD; PD = primary dendrites; CD = cell-form dendrites - B stands for Building direction and S for Laser scan direction

221 3.1.2. Inconel 625 obtained by LMD process

222 Figure 7 shows the Y-Z section images of the Inconel 625 sample fabricated
 223 by the LMD process. The microstructure appears to be also composed of cellular
 224 and primary dendrites. The cellular dendrites are often observed in the bottom
 225 part of each layer, near the melt pool limit.

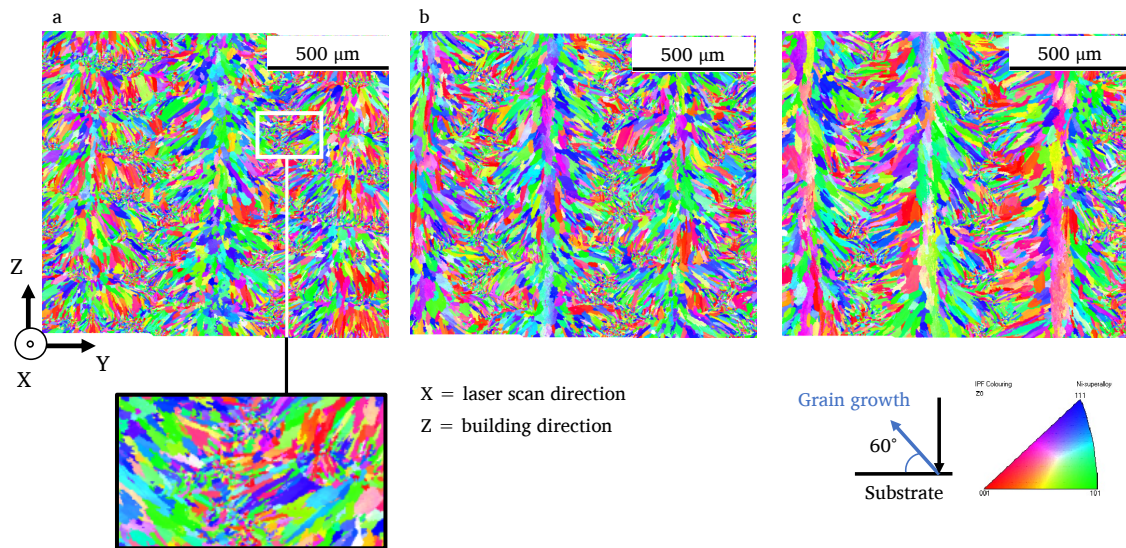


Figure 8: EBSD analyses of the LMD Inconel 625. Inverse pole figure (IPF) of the transverse section observations of samples printed at the same scan speed of $2500 \text{ mm}\cdot\text{min}^{-1}$ and different laser power. (a) 270 W; (b) 300 W; (c) 330 W.

226 Figure 8 presents the EBSD analyses of the Inconel 625 LMD samples. The
 227 IPF-Z images of the transverse section show a random texture of grains, contrary
 228 to the SLM samples. Strong differences in produced textures highlight an impor-
 229 tant relationship between the process and the microstructure. Indeed, the way the
 230 manufactured part is cooled down in the different processes is of primary impor-
 231 tance to understand the resulting microstructure. SLM parts are in direct contact
 232 with the supporting plane but also with the powder bed, reducing significantly the
 233 cooling rate as this latter acts as thermal insulator. In the contrary, for LMD spec-
 234 imens, there is an obvious vertical cooling toward the supporting plane but also
 235 heat exchanges with the ambient air and most especially an extra cooling coming
 236 from the last solidified layers beyond the melting bath. Dinda et al. [7] also
 237 states this hypothesis of shared cooling between the substrate and the adjacent

238 solidified layers in the case of a powder deposition manufacturing process, which
239 would cause grain growth at an angle of less than 90 compared to the substrate
240 and therefore a less pronounced texture. This weak texturing for LMD specimens
241 could therefore be related to a bidirectional growth of the dendrites grains. It has
242 been pointed out in the literature[7, 11], that the $\langle 001 \rangle$ preferential orientation
243 of grains is a consequence of the vertical heat flux direction, which imposes to the
244 primary dendrites a growth with an angle of about 90° with the substrate, which is
245 the case for SLM specimens . However, primary dendrites of each deposited layer
246 are not perpendicular to the substrate for LMD specimens. In our case, the grain
247 growth in each deposited layer converges to the center area, to form an inverted
248 "V" grain structure as shown in Figure 8. The angle of about 60 (also coherent
249 with values found by Dinda et al.), underlines that the vertical cooling to the sub-
250 strate could be twice as intense as the horizontal cooling flow via the previously
251 solidified zones.

252
253 Figure 8 also show the effect of the LMD manufacturing parameters on the
254 Inconel 625 microstructure. Here, all the manufacturing parameters indicated in
255 Table 3 were kept constant, except the laser power; three value are therefore in-
256 vestigated : 270W, 300W and 330W while the scan speed was taken constant at
257 2500 mm.min^{-1} . Results show that the laser power affects the size and the mor-
258 phology of the primary dendrites. For the minimal considered power value, 270
259 W, the primary dendrites appear to be finer than at 330 W. Furthermore, the lower
260 the laser power, the higher the ratio of small grains, located between deposit lines,
261 resulting of back and forth for the nozzle, appear.

262
263 These small grains are probably resulting from poorly melted powder or could
264 also be cellular dendrites, observed previously in Figure 7. At 330 W, the ratio
265 of small grains decreases greatly and the size of the primary dendrites increases.
266 These results might be explained by the rise of the melting temperature for the
267 powder with the laser power that could contribute to avoid poorly melted pow-
268 der. In the same way, a high temperature increases the local thermal heat flux,
269 which leads to much slower cooling rates and thus to significant dendritic growth
270 of grains for high laser powers.

271
272 Table 4 shows a statistical analysis of LMD samples microstructures obtained
273 from EBSD maps. For the grains detection, the indicated critical misorientation
274 is 15° and the grain filter (the minimum pixel area) for one grain is chosen at 3
275 pixels. Here, size of grains is first investigated and a threshold of 10 μm is cho-

Laser scan speed (mm/min)	Laser power (W)	Fraction surface of small grains* (for grain size < 10 μ m)	Ratio of dendritic structure (elongated grains : AR > 5)*
2500	270	12.2%	4.14%
	300	8.4%	4.72%
	330	3.6%	6.50%

Table 4: Effect of the manufacturing parameter (the laser power), on the grain size and the dendritic microstructure (*) : estimated on a $1.5 \times 1.5 \text{mm}^2$ area, from EBSD analyses.

276 sen to separate small and big grains (knowing that the average grain size for our
277 reference wrought sample is $15 \mu\text{m}$). In these conditions, results clearly denote a
278 decrease of the small grains fraction with the laser power. The ratio of dendritic
279 grains is also calculated, by considering the number of grains with an aspect ratio
280 greater than 5. The aspect ratio (AR) is a parameter which allows characterizing
281 the morphology of the grains from EBSD analyses. It corresponds to the ratio
282 between the large and the short length of the ellipse that fits best with the grain.
283 When the grain presents a perfect equiaxed form, AR is about 1, but this perfect
284 value stays unreachable in standard material. Therefore, grains AR distribution
285 is measured for our reference, the previously introduced wrought Inconel 625, to
286 know the repartition of equiaxed grains.

287

288 From results shown in Figure 9 and Figure 13.d, the AR critical value was
289 chosen equal at 5. Despite microstructure for wrought material is qualified of
290 equiaxial, the EBSD data of the as-received Inconel 625 reveal some annealing
291 twins, which present an elongated geometry with AR values more than 5. This
292 can explain the non-zero values of the AR distribution beyond 5. Thus, we as-
293 sume that for $\text{AR} > 5$, the grain shape could be considered as elongated for the
294 LMD samples. Then, the ratio of elongated grains is estimated in percent from
295 EBSD data to investigate the effect of the laser power. Results are presented in
296 Table 4. One can see that the increase of the laser power promotes the forma-
297 tion of elongated grains in the material. The laser power at 330W quicken the
298 dendritic growth of grains whose appear bigger than those at 270W and 300W
299 as observed on Figure 8. The microstructure seems once again narrowly linked
300 to the additive manufacturing process. Therefore, it seems necessary to consider
301 the effect of others manufacturing parameters such as the laser speed, the powder
302 flow rate, the scanning strategy, the nozzle increment in height, the powder qual-

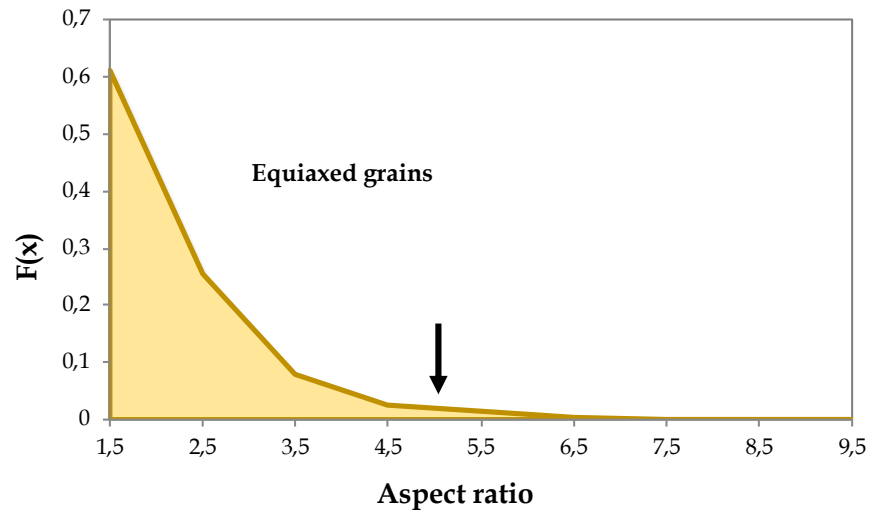


Figure 9: Aspect ratio distribution of grains in the wrought Inconel 625, showing the equiaxed grains repartition. The arrow indicates the critical value of the aspect ratio for an equiaxed structure.

303 ity and the substrate quality on the metallurgical rendering of the printed material.
 304 An optimization of these parameters should enable to reach a microstructure with
 305 a quality the nearest as possible as wrought material. Work is underway to then
 306 define more suitable parameters.

307 3.2. Effect of heat treatment on the microstructures

308 3.2.1. Our reference: wrought Inconel 625

309 First, the effect of heat treatment on the microstructure of the conventional
 310 Inconel 625 was investigated to study the phase transformations, independently
 311 of the additive manufacturing process. Our reference wrought Inconel 625 was
 312 heated at 600°C, 900°C and 1100°C, in a furnace during 1 hour, and then cooled
 313 in air.

314

315 It has been widely reported in the literature that Inconel 625 consists in an
 316 austenitic γ -Ni face-centered cubic solid solution, in which the intermetallic phases
 317 such as γ'' and δ are distributed in the grains and along the grain boundaries,
 318 respectively[5, 7]. Depending on the annealing temperature, the intermetallic
 319 phases γ'' and δ may precipitate in the matrix and affect the atoms rearrange-

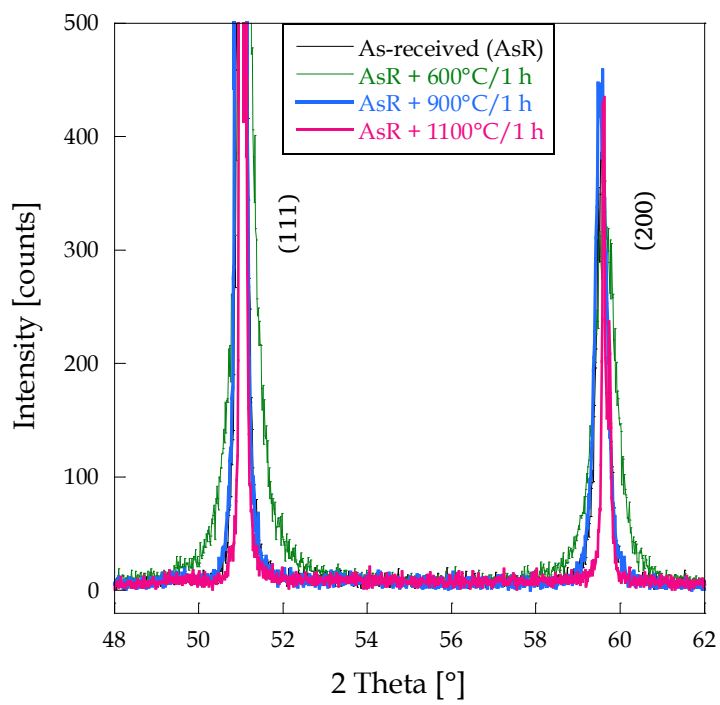


Figure 10: The (111) and (200) X-ray diffraction patterns of the wrought Inconel 625 sample annealed at different temperatures.

320 ment in the crystal lattice. X-Ray Diffraction (XRD) on the wrought samples
 321 under different heat treatments is commonly used[7, 11] to underline the appear-
 322 ance of a new phase in the austenitic matrix as the microstructure characterization
 323 is often difficult using standard techniques. Even if intermetallic phases are hardly
 324 detectable in the XRD diffraction patterns in reason of their small size[7], the vari-
 325 ation of the γ -Ni matrix lattice parameter can here indirectly imply the nature of
 326 precipitation. This lattice constant is calculated from the (200) diffraction peak as
 327 seen on Figure 10, according to the Bragg diffraction relation.
 328

Treatment of wrought Inconel 625	Lattice parameter(pm)
As-received	360.146
As-received + 600°C / 1h	359.546
As-received + 900°C / 1h	360.145
As-received + 1100°C / 1h	360.000

Table 5: Variation of the lattice parameter of the wrought Inconel 625 under different heat treatments.

329 Results are shown in Table 5 and are in accordance with previous studies
 330 [7, 11]. Without heat treatment, the strengthening elements such as Mo, Nb re-
 331 main in the γ -Ni matrix and cause a large lattice distortion. When the samples
 332 are heated at 600°C, the Nb atoms comes out of the matrix to form the γ'' pre-
 333 cipitates and the lattice parameter decreases correspondingly. As the temperature
 334 increases, the strengthening elements of precipitates are progressively dissolved
 335 into the matrix, leading to the increase of the lattice parameter. At 1100°C, while
 336 an increase in the lattice parameter was expected, a decrease is obtained. This
 337 observation can be explained by the presence of carbides precipitating from the
 338 matrix above 1000°C, as shown in literature[11, 12].
 339

340 Figure 10 shows the diffraction peak positions of the (111) and (200) crystal
 341 plane for different heat treatments. A broadening of these peaks can be observed
 342 after annealing at 600°C. The higher the annealing temperature, the narrower
 343 the integral line-breadth of the peaks becomes. Broadening of the XRD peaks
 344 is mainly attributed either to the crystallite size or to the increase of the micro-
 345 stresses in the material. In our specific case, we assume that the observed varia-
 346 tion comes from the micro-stresses. Micro-stresses are properties of the sample
 347 that result from the imperfections in the crystal lattice. These imperfections are

348 often associated with the local strains occurring on distances less than the crys-
349 tal dimensions. The precipitation of intermetallic phases in the austenite phase
350 could probably affect the atoms rearrangement in the lattice, leading to a small
351 deformation into the crystal lattice. The micro-stresses variation from one point
352 to another within the crystal lattice may alter the lattice spacing that causes the
353 broadening of the diffraction peak, as seen after annealing at 600°C. These as-
354 sumptions are corroborated by microscopic observations such as those shown in
355 the Figure 11. At 700°C, δ hardening precipitates in globular and acicular form
356 are observed. These precipitates gradually decrease at 900°C until they disappear
357 at 1100°C. These results were compared with those of Radavich et al.[5] with a
358 good consistency.

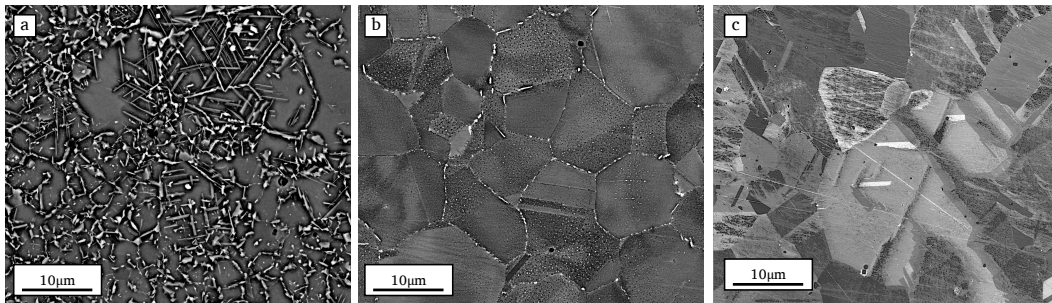


Figure 11: SEM images of wrought Inconel 625 samples annealed 1h a/ at 700°C; b/ at 900°C; c/ at 1100°C;

359 3.2.2. Inconel 625 obtained by SLM and LMD processes

360 Thereafter, thermal post-treatments were performed at 700°C, 900°C and 1100°C
361 to study the evolution of the dendritic structure observed previously for the SLM
362 and LMD samples. Figure 12 shows SEM images of samples heat-treated at these
363 temperatures. Observations reveal a constancy of the dendritic microstructure af-
364 ter annealing at 700°C for both processes (here only SLM results are presented).
365 The dendritic structure stays stable up to 900°C. At this point, the first steps of
366 the grains recrystallization take place with a widening of the dendrites grains as
367 shown in Figure 12.b for a SLM sample. However, these grains remain elongated
368 in the vertical plane and parallel to the build direction. When the SLM sam-
369 ples were annealed at 1100°C, the equiaxed grains start to appear with annealing
370 twins. These twinning highlight the release of the stored residual stress in the as-
371 built SLM sample, due to the high cooling rates during the building process[12].

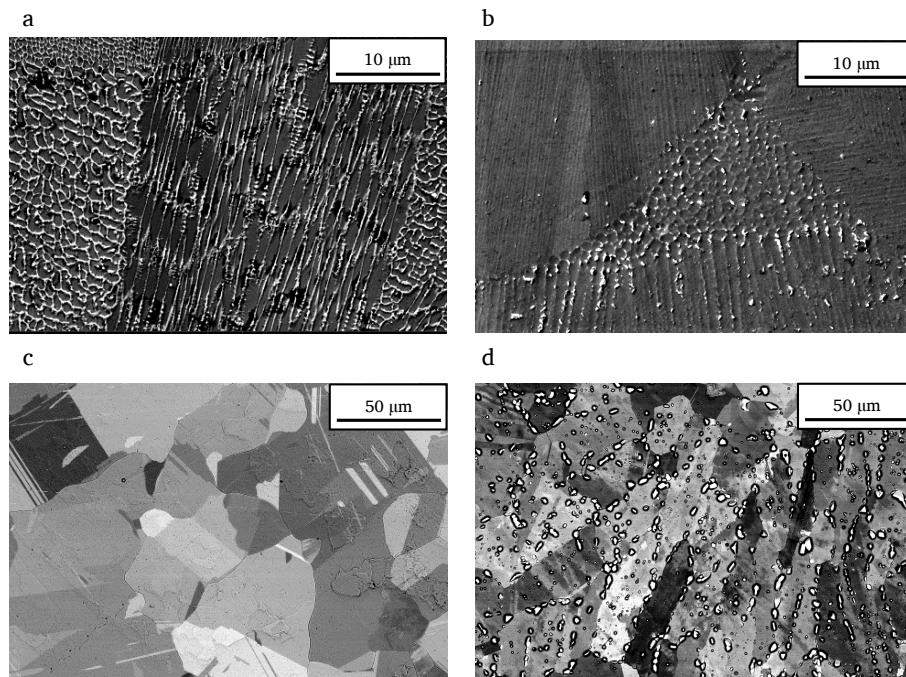


Figure 12: SEM images of the printed Inconel 625 samples annealed 1h at different temperatures. a/ SLM at 700°C; b/ SLM at 900°C; c/ SLM at 1100°C; d/ LMD at 1100°C

372 Figure 12.c reveals that the recrystallization process is achieved and there are no
373 dendritic grains after annealing at 1100°C for SLM samples, with a microstructure
374 which is close to the one obtained for wrought samples after 1h at 1100°C as seen
375 on Figure 11. Nevertheless, Figure 12.d shows that, in the case of a LMD sample
376 heat-treated during 1 hour at 1100°C, the microstructure consists in a mixture of
377 elongated and equiaxed grains, as an evidence that the recrystallization process is
378 here not completed. Dendrites inclination (about 60° with the substrate as seen on
379 Figure 8) observed in the as-built LMD sample and not in the SLM as-build sam-
380 ples, may explain these results. Further investigations should be here considered.
381 As stated for the wrought material, precipitates can also be observed during the
382 recrystallization process. The chemical nature of these precipitates was not stud-
383 ied in detail. Chlebus et al. performed EDS analyses in these interdendritic spaces
384 for an Inconel 718 and observed "small particles of eutectic mixture (δ +Laves-
385 type phase) and carbides" [19]. These results were also found in Antonsson et
386 al.[20]. Indeed, the high melting temperature during the process contributes to
387 raising concentrations of Nb, Mo, and C high enough to promote a rapid eutec-
388 tic reaction in interdendritic spaces[19], explaining the presence and evolution of
389 these precipitates with thermal history.

390
391 The EBSD maps in Figure 13 show the grains morphology of the as-built and
392 heat-treated LMD samples. It underlines that the elongated grains morphology,
393 specific to the dendritic microstructure, is found on the samples as-built and heat-
394 treated at 900°C (Figure 13.a and .b). In both cases, one can observed the inverted
395 "V" shape of the dendrites. As seen in Figure 13.c, the heat treatment at 1100°C
396 begins to eliminate the fine dendritic and columnar grains by recrystallization.
397 However, this annealing is not sufficient to obtain a homogeneous microstructure
398 compared to the as received wrought sample presented as a reference on Figure
399 13.d. Thus, the recrystallization process seems to be not complete after a heat
400 treatment of only one hour at 1100°C. For the wrought material, the grain size
401 distribution varies from 5 to 40 μ m, while for the LMD sample heat-treated at
402 1100°C/1 h, the range is from 5 to 180 μ m.

403 3.3. *Microhardness measurements*

404 Figure 14 shows the microhardness variation of the wrought, SLM and LMD
405 samples, as-built and heat-treated at 700, 900 and 1100°C for one hour. For the as-
406 built SLM and LMD specimens, the hardness values are 313 \pm 9 HV and 315 \pm 14
407 HV, respectively. These results are higher than those obtained for the wrought
408 sample, measured at 260 \pm 5 HV. The higher hardness of printed samples may be

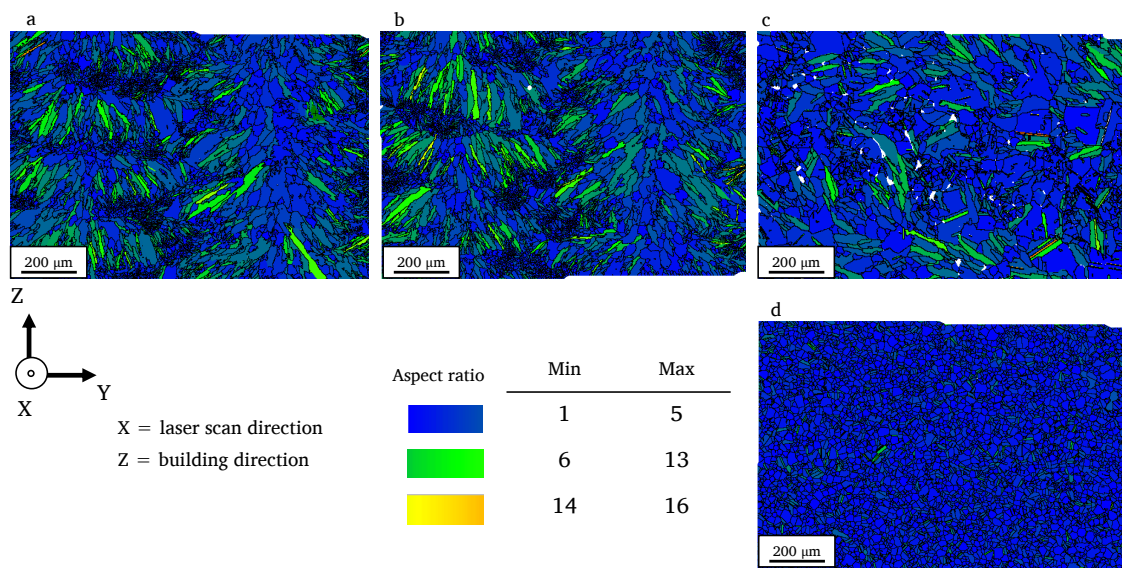


Figure 13: Grains morphology of LMD samples printed for a laser power of 270 W. (a) as built sample; (b) heat treated at 900C; (c) heat treated at 1100C; (d) for comparison, grains morphology of the wrought Inconel 625.

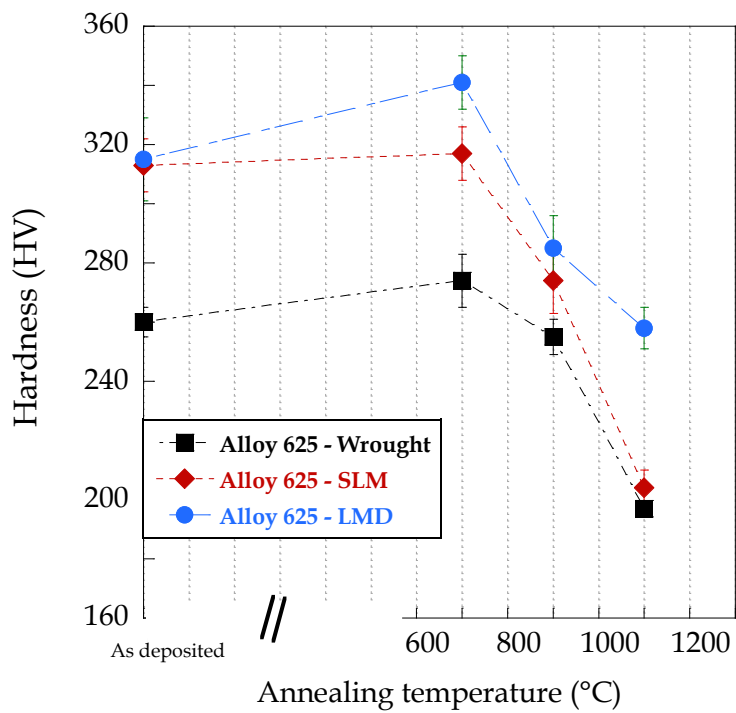


Figure 14: Hardness variation of Inconel 625 samples after annealing at different temperatures

409 explained by a potential high value for dislocation densities in the material result-
410 ing from the high cooling rate of the deposited layer during the printing process
411 ($10^5 K.s^{-1}$). Thus, the important solidification rate contributes to trap the heaviest
412 atoms, i.e. Nb and Mo, within the interdendritic areas, which may contribute to
413 increase the residual stresses in the as-built samples[12].

414

415 After post-annealing at $700^\circ C$, the hardness increases for all the samples: it
416 can be seen as a marker of the precipitation of the intermetallic phases γ'' in the
417 matrix. XRD results presented above are furthermore consistent with this conclu-
418 sion. Indeed, the hardening precipitates have been indirectly highlighted in the
419 γ -Ni matrix by the lattice parameter calculation in the case of the wrought sample
420 heat-treated at $600^\circ C$. As well, the decrease of the lattice parameter observed for
421 the sample annealed at this temperature could be explained by the precipitation
422 of $\gamma''[Ni_3Nb]$ phases resulting from the exit of Niobium atoms from the crystal
423 lattice [7].

424

425 For the SLM and LMD samples, heat treatment at $700^\circ C$ during 1h leads to
426 a hardness increase of respectively about 1% and 8%. Li et al [12] compared an
427 Inconel 625 processed by SLM before and after an heat treatment at $700^\circ C$ but
428 during 24h. They show that the release of segregation elements (Nb and Mo) en-
429 trapped in the interdendritic regions firstly leads to the decrease of the dislocation
430 density, but even more, causes the precipitation of more γ'' phases, increasing
431 slightly the hardness [12]. It seems here that the LMD sample heat-treated at
432 $700^\circ C$ for 1h also promotes the formation of more strengthening precipitates as
433 γ'' phases. The dendritic structure found on the LMD samples seems then to fa-
434 cilitate the departure of Nb and Mo elements, useful to form the strengthening γ''
435 phases, and thus increasing the measured hardness.

436

437 For the samples heat-treated at $900^\circ C$ and $1100^\circ C$, results show a decrease
438 of the hardness, certainly due to the progressive dissolution of the γ'' precipitates
439 in the matrix. In addition, at $1100^\circ C$, grain coarsening highly contributes to this
440 hardness lowering. However, the hardness of the LMD sample heat-treated at
441 $1100^\circ C$, remains higher than that of the wrought sample annealed at the same
442 temperature (see Figure 14). On the contrary, the hardness measurements are
443 almost similar for the SLM and wrought annealed specimens. In fact, it can be
444 seen on Figure 12 (d) that some precipitates were still present along the grain
445 boundaries of the LMD sample, despite the high temperature reached during the
446 heat treatments. MC and/or $M_{23}C_6$ carbides can then be seen as good candidate to

447 precipitate along the grain boundaries [12]. On the other hand, these precipitates
448 are not found for the SLM sample post-annealed at 1100°C as seen on Figure 12
449 (c). The strengthening effect of the LMD sample, heat-treated at 1100°C could
450 therefore be related to these carbides precipitates.

451 3.4. Tensile properties of Inconel 625

452 Tensile tests were first carried out on the as-received and the annealed-wrought
453 material. Two specimens were used to characterize each annealing condition and
454 the mean values of tensile properties are shown in Figure 15.

455

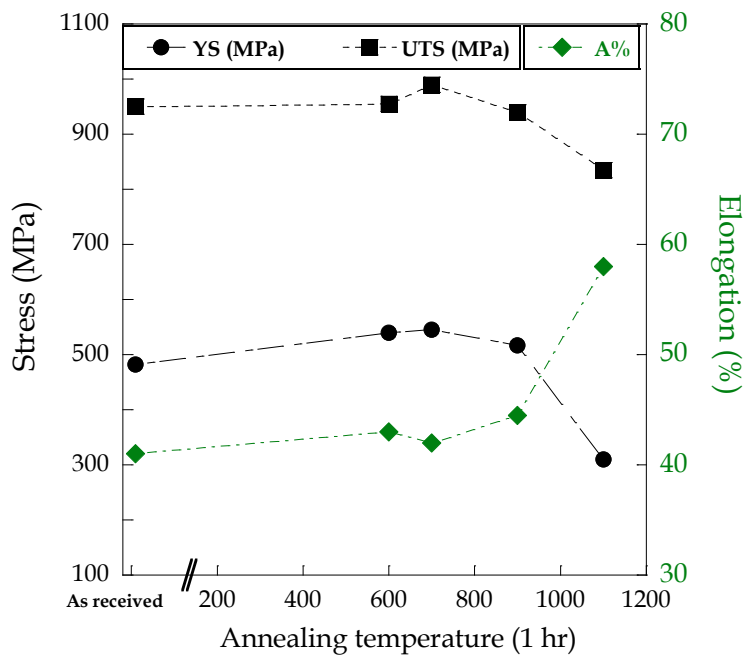


Figure 15: Tensile properties of the wrought Inconel 625 at different annealing temperatures

456 A small increase of the yield stress (YS) and the ultimate tensile strength
457 (UTS) is observed for specimens heat-treated at 700°C but this best-observed
458 strength characteristics (YS and UTS) are followed by a slight decrease of the
459 elongation to failure at this temperature, revealing that heat treatment at this tem-
460 perature range does not greatly affect the ductility of the material. These pretty

461 good tensile properties are probably due to the precipitation of the strengthening
 462 γ'' phases after exposure at temperatures between 600 and 700°C. Tensile
 463 strength characteristics (YS and UTS) then decrease as the heat treatment temper-
 464 ature increases. For specimens heat-treated at 900°C, this decrease is the result
 465 of a progressive dissolution of the precipitates in the matrix. Simultaneously, the
 466 ductility of the Inconel 625 heat-treated at 900°C and 1100°C increases gradually.
 467 The heat treatment was not optimized here because it was just a question of spec-
 468 ifying the influence of exposure to high temperatures on the material behavior in
 469 simple traction. Subsequently, a compromise can be sought in terms of heat treat-
 470 ment to obtain high tensile properties combined with good elongation to failure.

471

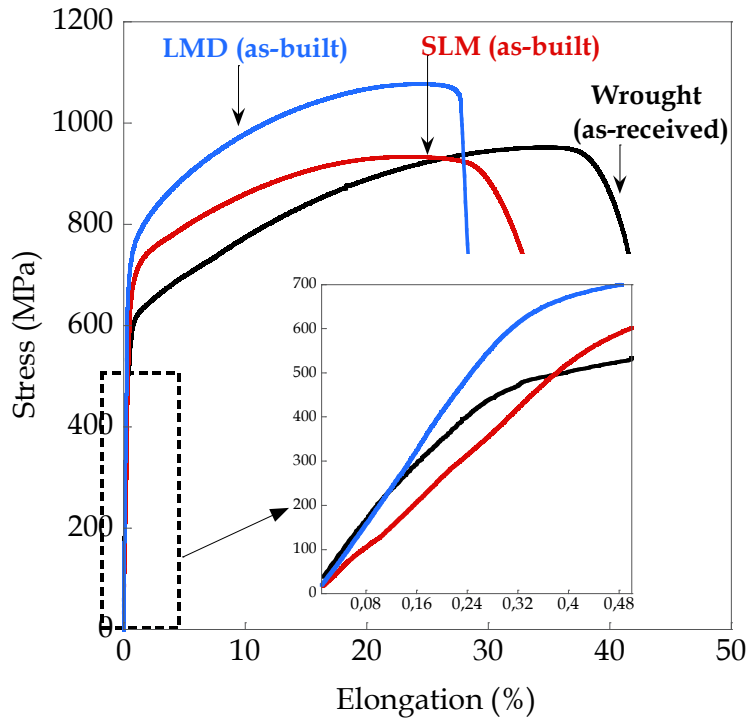


Figure 16: Tensile curves of Inconel 625. Comparison between the conventional and the additive manufacturing materials.

472 Concerning the AM specimens, the stress-strain tensile curves are shown in
 473 Figure 16. All the specimens were tested in the laser scan direction. A compari-
 474 son is established between the as-built AM specimens and the as-received wrought

475 material (commercial Inconel 625). Results show that the highest strength charac-
 476 teristics are obtained for the LMD specimens, with a YS 50% higher and an UTS
 477 12% higher than those of the wrought specimens. The SLM specimens present
 478 lower strength characteristics than those of the LMD (YS and UTS) but with a YS
 479 still 35% higher than the wrought material one for an even UTS. Strong differ-
 480 ences occur for the elongation to failure with SLM samples with a lower ductility
 481 than wrought material (22% mean drop) but higher than LMD specimens (37%
 482 drop on average compared to wrought material) (see Table 6) .

Inconel 625	Young Modulus (GPa)	Yield stress (MPa)	Ultimate tensile strength (MPa)	Elongation (%)
Wrought samples	184 ± 16	482 ± 42	955 ± 6	41 ± 1
<i>Samples processed by SLM</i>				
As-built (AS)	145 ± 4	652 ± 10	925 ± 13	32 ± 3
AS + 900°C/1 h	142 ± 11	567 ± 15	869 ± 7	38 ± 1
AS + 1100°C/1 h	114 ± 8	409 ± 14	886 ± 11	56 ± 5
<i>Samples processed by LMD</i>				
As-built (AS)	223 ± 24	723 ± 23	1073 ± 5	26 ± 2
AS + 900°C/1 h	224 ± 19	654 ± 15	1084 ± 2	27 ± 2
AS + 1100°C/1 h	213 ± 22	532 ± 22	991 ± 13	43 ± 1
<i>Other investigations</i>				
LMD [21]	-	656	1000	24
SLM [16]	182	783	1041	33
SLM [22]	196 ± 12	641 ± 24	879 ± 2	30 ± 2

Table 6: Tensile properties of Inconel 625

483 The inset in 16 shows a magnification of the tensile curves between 0 and
 484 0.5% of mechanical strain. It is interesting here to compare the elastic behavior
 485 of AM and wrought specimens. Results indicate a lower Young modulus for the
 486 specimens printed by the SLM process. Moreover, the elastic evolution of LMD
 487 and wrought specimens seems more similar. These observations suggest that me-
 488chanical properties for the as-built SLM and LMD specimens are different. This
 489 may be certainly explained by the strong differences in terms of microstructure or
 490 by the dislocations structures, resulting from difference in the process. Concern-
 491 ing the microstructure, the EBSD analysis of the SLM specimens indeed shows a
 492 very strong texture, with a preferential orientation $\langle 001 \rangle$, as for a single crystal

493 material. In this case, the low slope of the stress-strain curve indicates that the acti-
 494 vation of the sliding systems for plasticity proper to the cubic faced-centered (cfc)
 495 structure would be faster in the as-built SLM specimens : this hypothesis could
 496 be tested by modifying the printing strategy of SLM specimens, which would be
 497 a study in itself.

498

499 Table 6 also summarizes the literature results of tensile tests realized on hori-
 500 zontal Inconel 625 processed by additive manufacturing. For the as-built LMD
 501 sample, obtained tensile properties are practically similar to the literature investi-
 502 gation [21]. Moreover, the authors also obtained a mixed dendritic and columnar
 503 microstructure with cellular and elongated grains, in line with our observations.
 504 For the SLM samples, the elongation to failure was found closed to the literature
 505 observations [16, 22]. Nonetheless, Marchese et al.[16] determined higher tensile
 506 strengths, which can be related to the less-pronounced grains texture. Once again,
 507 the preferred $\langle 001 \rangle$ grains orientation presented in this paper seems to explain
 508 the low value of the Young modulus and yield stress of the as-built SLM sample.

509

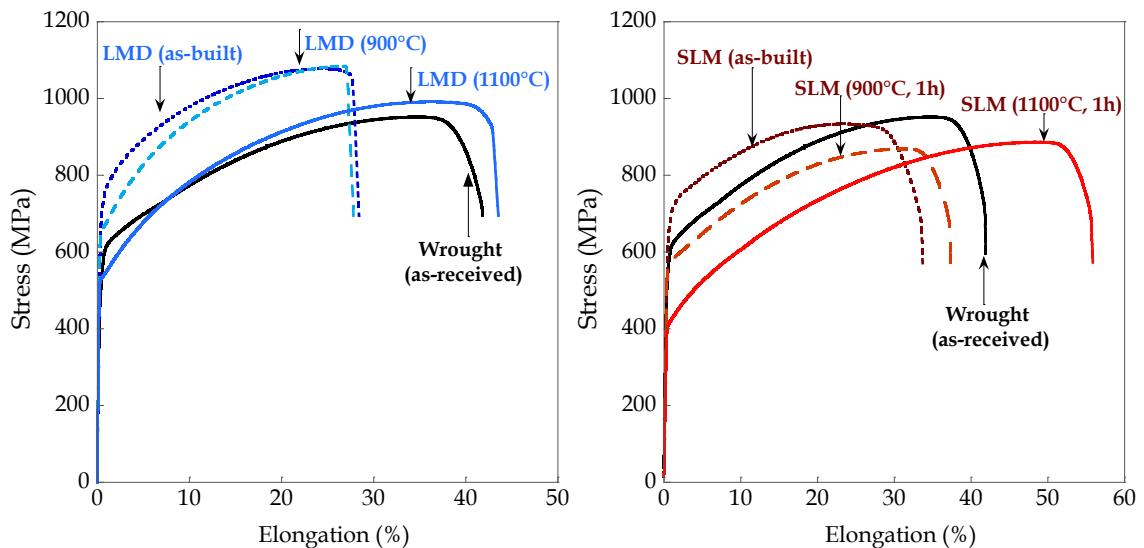


Figure 17: Effect of heat treatments on tensile properties of Inconel 625 for the LMD samples (in blue); for the SLM samples (in red).

510 After heat treatment, the YS and UTS for the LMD specimens are still higher
 511 than those of the wrought sample (see Figure 17.a). Compared to the as-built

512 LMD specimens, there is no significant change on the ultimate strength and the
513 elongation to failure after the annealing at 900°C (Table 6). However, YS de-
514 creases slightly, probably due to the beginning of the residual stresses relaxation
515 during the post-annealing treatment. After annealing at 1100°C , the mechanical
516 strengths of the LMD specimens decrease again, while the elongation to failure
517 increases. As shown in Table 6, the mechanical properties of the LMD samples
518 heat-treated at 1100°C become similar to those of the conventional wrought ma-
519 terial. Moreover, the obtained UTS and elongation values turn out to be slightly
520 higher. This heat treatment favors the improvement of the ductility that increases
521 by up to 65% compared to the as-built state and provide a material which is close
522 to the wrought one.

523

524 On the other hand, for SLM specimens, heat treatment at 900°C greatly affects
525 the tensile properties. YS decreases by 13% compared to the as-built state, while
526 the elongation to failure increases by 19%. As shown in Table 6, the annealing at
527 1100°C allows here again an improvement of ductility, which increases by 75%
528 compared to the as-build material and reaches 43%. The mechanical strengths of
529 the SLM specimens annealed at 1100°C however become lower than the conven-
530 tional wrought Inconel 625. Here, a more in-depth investigation should be carried
531 out to find the most suitable heat treatment to obtain interesting properties for the
532 SLM material. It is thus important to note that simple exposure to high tempera-
533 tures is not sufficient enough to improve SLM material properties.

534

535 It is finally interesting to stress out the effect of texture and the influence of the
536 loading direction. Elongated grains in the preferred $\langle 001 \rangle$ orientation for SLM
537 specimens are here perpendicular to the mechanical stress direction, which favors
538 a faster activation of the micro-plasticity sites and therefore leads to a decrease for
539 the mechanical resistance compared to LMD specimens. Such texture effect has
540 been previously pointed out by Ma et al. [23]. The apparent observed ductility
541 for printed specimens are lower for example essentially because the failure will
542 come faster partially because of the strong texture effect. Nevertheless, if the
543 direction of loading is parallel to the grain orientation, then the tensile properties
544 should be better; Kreitchberg et al [17] indeed shows that the ductility for Inconel
545 625 specimens obtained by LMD is better when they are printed vertically than
546 horizontally. For LMD samples, the more homogeneous texture surely makes the
547 material less sensitive to loading direction. Once again, further investigations on
548 texture and precipitates effect on mechanical properties have to be performed.

549 4. Some discussions

550 The analysis of the previous results underlines that the high cooling rate which
551 occurs during the additive manufacturing processes affects the grain morphology
552 and the texture of printed parts. It is shown that the grains usually appear more
553 elongated in the direction parallel to the build direction. A dendritic growth was
554 therefore identified from the bottom to the top part of the melt pool. As shown
555 previously, the bottom part of the layer mostly consists of columnar structure with
556 cell-form dendrites, while the top part of the layer shows a very fine dendritic
557 structure. This is a consequence of the downward progressive solidification ve-
558 locity, which is higher at the bottom zone than at the upper one. The main pa-
559 rameters piloting the LMD manufacturing process have thus a substantial impact
560 on the size and the morphology of the grains. A high laser power contributes to
561 a significant formation of elongated grains, which also appear bigger, whilst the
562 number of cell-form dendrites decrease. Indeed, a part of the laser power may be
563 absorbed by the powder and used to bring it to temperature and generate melt pool.
564 The laser-deposited layer is then subjected to a non-isothermal annealing (without
565 temperature maintain) which greatly influences the phase transformations and the
566 recrystallization processes during the manufacturing phases. Thus, the average
567 temperature of the laser-deposited layer is going to decrease gradually, depend-
568 ing on its vicinity to the substrate. The farther the layer from the substrate, the
569 lower the cooling rate [17]. Thereby, an increase in the laser power would result
570 in a greater heat flux that may promote the formation of a hugely dendritic mi-
571 crostructure with elongated grains.

572
573 To go a bit further, this global "macroscopic" influence of this laser power
574 is finally briefly investigated. Figure 18 illustrates the correlation between this
575 manufacturing process parameter and both the microstructure and the mechani-
576 cal properties of parts printed by LMD. For each of the parameters studied, the
577 material with the highest value is given a maximum score of 1, so that the score
578 for the other materials is deduced by a simple rule of three from this reference.
579 The effect of laser power on the microstructure (ratio of elongated grains) is here
580 obvious and highlighted by the increase of the dendritic structure with power. It
581 is however less significant on the hardness and the yield stress. The maximum
582 hardness is obtained for the printed part at 270W : 343 ± 9 HV, while the mini-
583 mum hardness is 315 ± 14 HV, for a 300W laser power. For the yield stress, the
584 maximum value was also obtained for the sample printed at 270W (746 MPa),
585 and similar values were found for 300W and 330W. Therefore, it seems that the

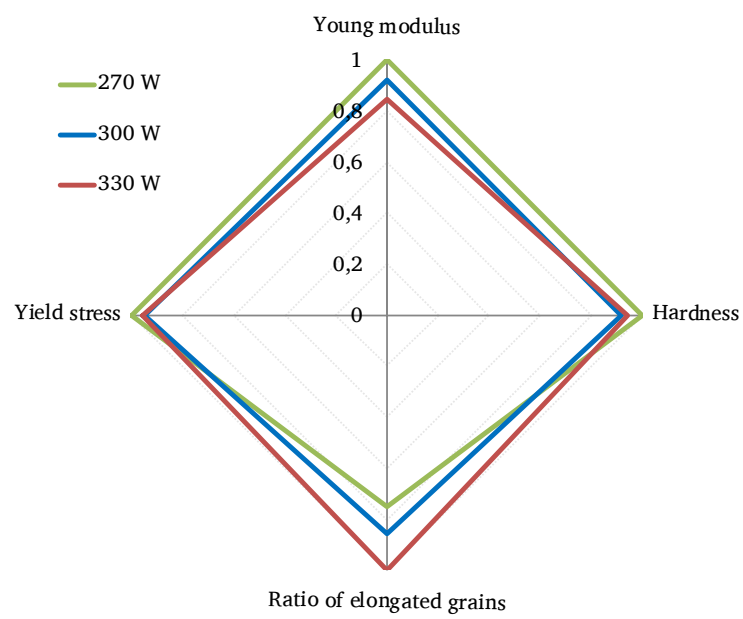


Figure 18: Correlation between the laser power of the manufacturing process, the microstructure and the mechanical properties of Inconel 625 obtained by LMD

586 elongated grains morphology does not play a significant part on the improvement
 587 of the mechanical properties for horizontally-printed bars.

588

589 Finally, the Young modulus also shows its maximum value (239 GPa) at the
 590 lowest laser power. with significant variations with a decrease of nearly 20% at
 591 330W. These results thus emphasize a significant effect of the laser power on the
 592 microstructure, among others, on the morphology and orientation of the grains
 593 which in turn lightly affects the mechanical properties of the LMD printed parts
 594 (for example, no variation on the elongation to failure was detected for samples
 595 printed at 270, 300 and 300W).

596

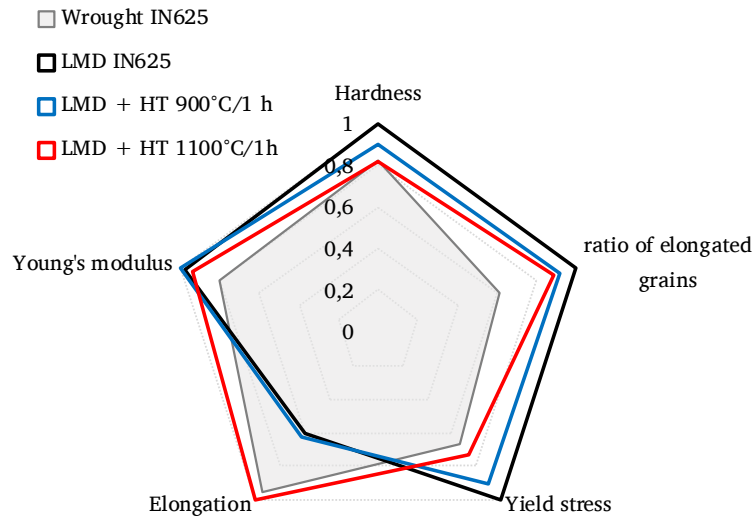


Figure 19: Effect of post-annealing treatments on the microstructure and mechanical properties of LMD samples.

597 Figure 19 finally shows the impact of the post-annealing treatment on the mi-
 598 crostructure and mechanical properties of samples processed by the LMD. Compar-
 599 ing to the conventional wrought material, one can see that the heat-treatment
 600 performed at 1100°C contributes to reduce the high value for hardness obtained
 601 for the LMD as-built material, due to residual stresses. After 1h at this temper-
 602 ature, it tends to be similar to the wrought material one. In the same way, this
 603 post-treatment improve the grains morphology by the recrystallization process to

604 achieve an equiaxed grains microstructure close to the traditional material one.
605 The duration of the heat-treatment at 1100°C seems however to be rather low to
606 fully homogenize the size and the grains shape. One can also see that the strengths
607 and the Young modulus of the LMD samples are much higher than the conven-
608 tional wrought, even after the heat treatment. As a result, the post-annealing seems
609 to be the most effective way to greatly improve the ductility of AM parts, while
610 keeping good tensile strengths and finally obtain an improved printed material if
611 compared with the wrought one.

612 **5. Conclusion**

613 The microstructure characteristics as well as the mechanical properties of an
614 Inconel 625 alloy obtained by three processes: forging, SLM and LMD, were
615 studied. For the last two processes, known as "additive manufacturing", the in-
616 fluence of printing parameters was considered as well as the role of possible heat
617 treatments. The main conclusions of this study are :

- 618 • Additive Manufacturing processes induce the presence of columnar den-
619 drites with a very heterogeneous grain size for as-built materials.
620
- 621 • The microstructures appear highly textured with a privileged grain orienta-
622 tion, particularly for SLM: the material is thus very far from the equiaxed
623 microstructure of the wrought alloy.
624
- 625 • The microstructure obtained by SLM is often finer than the one obtained by
626 LMD even if a reduction in laser power tends to refine it.
627
- 628 • Heat treatments and particularly the 1h- 1100°C annealing enable to improve
629 the printed parts microstructure by suppressing the columnar dendrites
630
- 631 • The hardness and tensile properties of the printed parts (yield stress and ten-
632 sile strenght) are most of the time better than that of wrought parts but their
633 ductility is often low.
634

- 635 • Annealing at 1100°C improves the ductility: all the mechanical properties
636 of the LMD material become closer to those of the wrought one.
- 637 • The LMD process with controlled laser power, coupled with appropriate
638 heat treatment, produces both microstructures and mechanical properties
639 close to or better than those of the wrought alloy.

640 Finally, some complementary investigations could be done in order to improve
641 the microstructural characteristics of the as-built Inconel 625, by looking for a
642 series of adequate parameters to achieve a more homogeneous behavior for printed
643 material. The study of the fatigue strength of this type of printed alloy can also be
644 an interesting property to investigate.

645 **6. Acknowledgements**

646 The authors thank the French Délégation Générale pour l'Armement (DGA)
647 for funding this study and Eric Lafontaine for fruitful discussion. The FEG SEM
648 FEI Quanta 600 has been acquired with the financial support of Region Ile-de-
649 France (SESAME 2004 program), CNRS, and Ecole Polytechnique. Finally, the
650 authors also gratefully acknowledge Loïc Perrière from ICMPE for his help with
651 XRD.

652 **7. Data availability**

653 The raw/processed data required to reproduce these findings cannot be shared
654 at this time as the data also forms part of an ongoing study

655 **8. References**

- 656 [1] Vernot-Loier C., Cortial F., *Superalloys 718, 625 and various derivatives*,
657 in: E. A.Loria (Ed.), *Superalloys 718, 625 and Various Derivatives*, TMS,
658 Pittsburgh, PA, USA, 1991, pp.409-422.
- 659 [2] Shankar V., Rao K., Mannan S.L., *Microstructure and mechanical properties*
660 *of Inconel 625 superalloy*. *Journal of Nuclear Materials* (2001) 288 222-232.
- 661 [3] Zhang B., Bi G, Wang P, Bai J, Chew Y, Nai MS. *Microstructure and*
662 *mechanical properties of Inconel 625/nano-TiB2 composite fabricated by*
663 *LAAM*. *Materials & Design* (2016) 111: 70-79

- 664 [4] Liu M, Zheng W, Xiang J, Song Z, Pu E, Feng H. *Grain Growth Behavior*
665 *of Inconel 625 Superalloy*. Journal of Iron and Steel Research International
666 (2016) 23 (10): 1111-1118.
- 667 [5] Radavich J.F., Fort A. *Effects of Long-Time Exposure in Alloy 625 at 1200F,*
668 *1400F and 1600F*. Paper presented at Superalloys 718, 625 and Various
669 Derivatives, TMS, Pitts-burgh, PA, USA, 1994, pp.635-647.
- 670 [6] M. Khler. *Effect of the elevated-temperature-precipitation in Alloy 625 on*
671 *properties and microstructure*. Paper presented at Superalloys 718, 625, 706
672 and Various Derivatives, TMS, Pittsburgh, PA, USA, 1991, pp. 363-374.
- 673 [7] Dinda, G.P., Dasgupta, A.K., and Mazumder, J. *Laser aided direct metal*
674 *deposition of Inconel 625 superalloy: Microstructural evolution and thermal*
675 *stability*. Materials Science and Engineering A (2009) 509: 98-104
- 676 [8] Sandhu SS, Shahi AS. *Metallurgical, wear and fatigue performance of*
677 *Inconel 625 weld claddings*. Journal of Materials Processing Technology
678 (2016) 233: 1-8
- 679 [9] Frazier W. E., *Metal Additive Manufacturing: A Review* Journal of Materials
680 Engineering and Performance 2014, 23, 1917.
- 681 [10] Marchese, G., Garmendia, X., Calignano, F., et al. *Characterization and*
682 *Comparison of Inconel 625 Processed by Selective Laser Melting and Laser*
683 *Metal Deposition*. Advanced Engineering Materials 2017, 19, No. 3, p.1-9
- 684 [11] Li, S., Wei, Q., Shi, Y., Zhu, Z., and Zhang, D. *Microstructure Character-*
685 *istics of Inconel 625 Superalloy Manufactured by Selective Laser Melting*.
686 Journal of Materials Science & Technology (2015) 31, 946-952
- 687 [12] Li C., White R., Fang X.Y., Weaver M., Guoa Y.B. *Microstructure evolu-*
688 *tion characteristics of Inconel 625 alloy from selective laser melting to heat*
689 *treatment*. Materials Science & Engineering A (2017), 705: 20-31
- 690 [13] Hack, H., Link, R., Knudsen, E., Baker, B., and Olig, S. *705 Mechanical*
691 *properties of additive manufactured nickel alloy 625*. Additive Manufactur-
692 ing 705, 14, 105-115

- 693 [14] Rivera O.G., Allison P.G., Jordon J.B., Rodriguez O.L., Brewer L.N., Mc-
694 Clelland Z., Whittington, W.R., Francis, D., Su, J., Martens, R.L., et al. *Mi-*
695 *crostructures and mechanical behavior of Inconel 625 fabricated by solid-*
696 *state additive manufacturing*. *Materials Science and Engineering: A* (2017),
697 694, 1-9
- 698 [15] Amato, K., Hernandez, J., and Murr, L.E. *Comparison of Microstructures*
699 *and Properties for a Ni-Base Superalloy (Alloy 625) Fabricated by Electron*
700 *Beam Melting*. *Journal of Materials Science Research* (2012a): 1, 3-41.
- 701 [16] Marchese G., Lorusso M., Parizia S., Bassini E. et al. *Influence of heat treat-*
702 *ments on microstructure evolution and mechanical properties of Inconel 625*
703 *processed by laser powder bed fusion*. *Materials Science & Engineering A*
704 (2018) 729: 64-75
- 705 [17] Kreitchberg A., Brailovskia V., Turenneb S. *Effect of heat treatment and hot*
706 *isostatic pressing on the microstructure and mechanical properties of In-*
707 *conel 625 alloy processed by laser powder bed fusion*. *Materials Science &*
708 *Engineering A* 689 (2017) 1-10
- 709 [18] Verdi, D., Garrido, M.A., Mnez, C.J., and Poza, P. *Mechanical properties*
710 *of Inconel 625 laser clad coatings: Depth sensing indentation analysis*.
711 *Materials Science and Engineering: A* 598, (2014) 15-21.
- 712 [19] Chlebus, E., Gruber, K., Kuznicka, B., Kurzac, J., Kurzynowski, T. (2015).
713 *Effect of heat treatment on the microstructure and mechanical properties of*
714 *Inconel 718 processed by selective laser melting*. *Materials Science and En-*
715 *gineering: A*, 639, 647-655.
- 716 [20] Antonsson, T., Fredriksson, H. (2005). *The effect of cooling rate on the so-*
717 *lidification of INCONEL 718*. *Metallurgical and Materials Transactions B*,
718 36(1), 85-96.
- 719 [21] Rombouts M., Maes G., Mertens M., and Hendrix W., *Laser metal depo-*
720 *sition of Inconel 625: Microstructure and mechanical properties*. *J. Laser*
721 *Appl.* 24 (2012) 52007.
- 722 [22] Wang P., Zhang B., Tan C.C., Raghavan S., Lim Y.-F., Sun C., et al. *Mi-*
723 *crostructural characteristics and mechanical properties of carbon nanotube*
724 *reinforced Inconel 625 parts fabricated by selective laser melting*. *Mater.*
725 *Des.* 112 (2016) 290-299

- 726 [23] Ma, D., Stoica, A. D., Wang, Z., Beese, A. M. (2017). Crystallographic tex-
727 ture in an additively manufactured nickel-base superalloy. *Materials Science*
728 *and Engineering: A*, 684, 47-53.